Current Biology, Vol. 12, 383–388, March 5, 2002, ©2002 Elsevier Science Ltd. All rights reserved. PII S0960-9822(02)00678-4

Each Actin Subunit Has Three Nebulin Binding Sites: Implications for Steric Blocking

Natalya Lukoyanova,[1] Margaret S. VanLoock,[1] Albina Orlova,[1] Vitold E. Galkin,[1] Kuan Wang,[2] and Edward H. Egelman[1,3]

[1]Department of Biochemistry and Molecular Genetics
University of Virginia
Charlottesville, Virginia 22908-0733
[2]Laboratory of Muscle Biology
National Institute of Arthritis and Musculoskeletal and Skin Diseases
National Institutes of Health
Bethesda, Maryland 20892

Summary

Nebulin is a giant protein that spans most of the muscle thin filament [1, 2]. Mutations in nebulin result in myopathies and dystrophies [3, 4]. Nebulin contains ~200 copies of ~35 residue modules, each believed to contain an actin binding site, organized into seven-module superrepeats [5, 6]. The strong correlation between the number of nebulin modules and the length of skeletal muscle thin filaments in different species suggests that nebulin determines thin filament length [2, 7, 8]. Little information exists about the interactions between intact nebulin and F-actin. More insight has come from working with fragments of nebulin, containing from one to hundreds of actin binding modules. However, the observed stoichiometry of binding between these fragments and actin has ranged from 0.4 to 13 modules per actin subunit [9–12]. We have used electron microscopy and a novel method of helical image analysis to characterize complexes of F-actin with a nebulin fragment. The fragment binds as an extended structure spanning three actin subunits and binding to different sites on each actin. Muscle regulation involves tropomyosin movement on the surface of actin, with binding in three states. Our results suggest the intriguing possibility that intact nebulin may also be able to occupy three different sites on F-actin.

Results and Discussion

We have used ND66 [6, 10], a cloned nebulin fragment from the C terminus of human fetal nebulin (Figure 1). Depending upon the choice of phasing [6, 13], this fragment contains either three or four actin binding modules. Incubation of the ND66 fragment with F-actin results in the presence of both free filaments (Figure 2C) as well as "rafts" of parallel filaments (Figure 2B). The lateral spacing of filaments within these rafts was quite variable, but a mean distance of ~160 Å was measured in regions where filaments were fairly ordered. We interpret these rafts as arising from the same ND66 fragment binding to adjacent filaments, using the multiple actin binding sites contained within ND66. Image analysis of the more ordered regions of parallel filaments failed to detect any feature between filaments that might be due to the ND66 fragment. However, this would be consistent with an extended structure for ND66, and the mass between actin filaments would therefore be very small in contrast to the mass seen when globular proteins such as fimbrin [14], fascin [15], or scruin [16] bundle actin filaments. The crosslinking of actin filaments by ND66 is very similar to the previous observation that a nebulin fragment containing six modules bundled F-actin [11].

Electron micrographs of isolated actin:ND66 filaments (Figures 2B and 2C) were analyzed using an iterative helical real space reconstruction (IHRSR) method [17] that surmounts the problem of both variable twist in F-actin [18] and incomplete or disordered decoration of F-actin by ND66. Previous applications of this method to complexes of actin and Actin Depolymerizing Factor (ADF) were very successful in finding two different modes of binding of ADF to actin [18], and these modes would have been difficult or impossible to separate by conventional methods of helical image analysis [19]. The method has recently been applied to actin filaments with an engineered intersubunit disulfide bridge [20] and has also been used to successfully sort segments of RecA-DNA [21], UvsX-DNA [22], and RadA-DNA [23] filaments by both helical pitch and structure. Thus, the method has been extensively tested. Images of ~32,000 filament segments were repeatedly sorted into two classes, one containing pure F-actin and the other ND66-decorated F-actin, using improved reconstructions of the F-actin:ND66 complex each cycle. The final sorting placed ~62% of the filament segments in the undecorated category and ~38% in the ND66-decorated group (Figure 3C). Since segments with partial occupancy by ND66 or with different modes of binding by ND66 may end up being classified as undecorated, these percentages cannot be directly interpreted in terms of an overall stoichiometry of binding. In fact, the main effect of the sorting may very well be in eliminating ND66 fragments that are bound in a disordered manner, to yield a reconstruction where the mass due to ND66 is now very clearly visible. In contrast, there have been previous reconstructions of F-actin with actin binding proteins using helical averaging where parts or even most of the density due to the actin binding protein is not fully seen [24, 25]. The additional mass due to the ND66 fragment (Figures 3D and 3E) was judged to be highly significant and extremely reproducible using different starting points for the three-dimensional reconstruction. Several differences were observed in the actin itself in the comparison between the decorated and undecorated reconstruction. The density due to subdomain 2 of actin is not seen in the reconstruction of the fully decorated filaments, but this is consistent with numerous previous observations showing that this is the most variable part of the actin structure [26]. There is an apparent closing of the nucleotide binding cleft after decoration by ND66, but this is

[3]Correspondence: egelman@virginia.edu

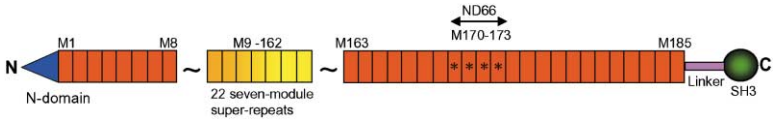

Figure 1. Nebulin Domain Architecture

Human adult nebulin consists of four domains: an acidic N-terminal domain (blue); 185 copies of ~35 residue nebulin modules (M1–185) that are either single repeats (M1–8, M163–185, red) or seven-module superrepeats (M9–162, orange-yellow); a serine-rich linker (magenta); and a SH3 domain (green) at the C terminus [5]. Each single nebulin molecule extends from the pointed end of thin filaments (N terminus) to the Z line (C terminus) in the muscle sarcomere [2, 5, 48]. ND66 is a 128 residue fragment in the highly homologous single-repeat segment near the C terminus of human fetal nebulin [6], contains four 31 residue nebulin modules, and corresponds closely to the M170–173 sequence of human adult nebulin (accession number X83957 [5]). This single repeat region is found near the edge of the Z line in the sarcomere and binds actin, tropomyosin, troponin, calmodulin [6], and desmin [49].

also consistent with known internal modes of G- and F-actin [27, 28]. The changes that are seen in subdomains 3 and 4 (Figure 3D) may be associated with this closing of the cleft.

Further confidence in the reconstruction comes from using ND66 to polymerize F-actin. It has previously been shown that nebulin fragments can act as potent nucleators of F-actin assembly [11, 29]. Approximately 28,000 segments were selected from filaments formed when G-actin was polymerized by the addition of ND66 under low-salt conditions where the G-actin does not spontaneously polymerize (Figure 2D). These segments were sorted in the same manner as those from F-actin decorated with ND66 and yielded a distribution of ~56% undecorated and ~44% ND66 decorated. Given the caveats discussed above, these numbers cannot be directly interpreted in terms of a stoichiometry of binding. Reconstructions from the decorated ND66-G-actin segments (Figure 3B) were similar to the reconstructions of decorated F-actin in the pattern of binding by ND66 but showed less additional mass. We interpret this as simply less complete decoration. In addition, reconstructions were generated for both sets (decorated F-actin and decorated ND66-polymerized G-actin) from segments sorted into different helical symmetries (with twists from 162°–167° per actin subunit), and all showed the same general features.

The reconstructions did not show a single continuous density for this nebulin fragment binding to each actin subunit. Rather, three sites of additional mass were found on each actin subunit. When surfaces were examined at lower thresholds (Figures 4D and 4F), the additional densities were seen to be connected and could be explained by an ND66 molecule that binds to three actin subunits. Using a single α helix to model ND66, it was found that the additional densities in the reconstruction could be completely explained (Figures 4C and 4F) by an ND66 fragment that bound to subdomain 1 of one actin subunit, a different site on subdomain 1 of an actin subunit below it, and then subdomain 4 of an actin subunit on the opposite long-pitch helical strand. Thus, each fragment binds to three actin subunits, and the binding appears to involve three different ND66 fragments bound to each actin subunit at three different

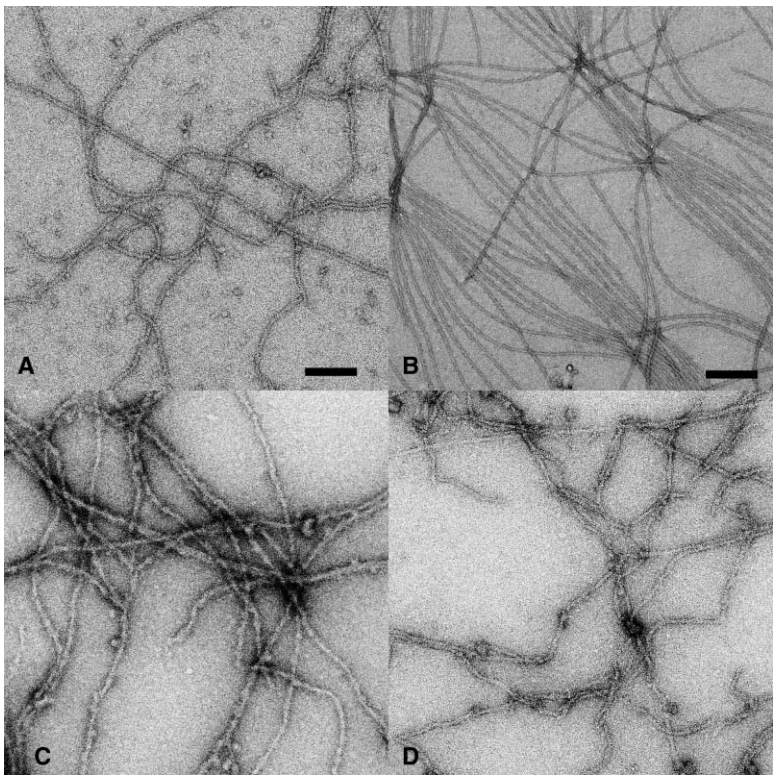

Figure 2. Electron Micrographs of Actin and Actin-ND66 Complexes

Pure F-actin (A), F-actin incubated with the ND66 fragment (B and C), and G-actin polymerized with ND66 under low-salt conditions (D). Rafts of parallel actin filaments can be seen (B) after incubation of F-actin with ND66, but similar rafts are not seen in control F-actin (A) or when G-actin is polymerized by ND66 (D). The scale bar in (A) is 1000 Å and applies to (A), (C), and (D), while the scale bar in (B) is 2000 Å.

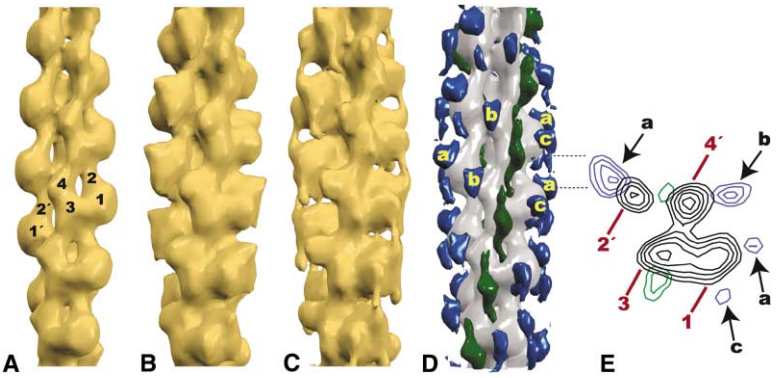

Figure 3. Reconstructions of Actin and Actin-ND66 Filaments

Surfaces from undecorated F-actin (A), decorated segments of G-actin polymerized by ND66 (B), and ND66-decorated F-actin (C). A statistical difference map between ND66-decorated F-actin (C) and undecorated F-actin (A) is shown as a surface (D) and in a contour plot (E), superimposed on the undecorated actin. The position of the slice shown in (E) is indicated in (D) by either of the dashed lines (every slice spaced ~27 Å apart will be identical but rotated by ~166°). The threshold for the t map in (D) and (E) is 4.0, with a step size of 4.0 between contours in (E). The differences due to ND66 are labeled as "a," "b," and "c" in (D) and (E) and are shown in blue. The differences due to a change in actin are shown in green (D and E). The peak of the difference due to ND66 has a t value of ~18, while that due to a change in actin has a peak of ~12. The differences shown correspond to the regions where the actin-ND66 map is greater in density than the undecorated actin map. The negative differences mainly involve subdomain 2, since the density due to this subdomain is not seen in the decorated map. An additional negative difference is seen in the region of the C terminus. The actin subdomains 1 through 4 are labeled in (A), and subdomains 1 and 2 from a different subunit are labeled 1′ and 2′. The subdomains 1 and 3 from one subunit are labeled in (E), and subdomains 2 and 4 from a different subunit are labeled 2′ and 4′ in (E). The surface in (A) is shown at ~100% of the expected molecular volume, the surface in (B) at ~120%, and the surface in (C) at ~115%.

sites. None of the three sites is consistent with a previously postulated model for nebulin binding in the groove between the two long-pitch actin strands [30]. Instead, two of the three observed sites are consistent with a model where nebulin is attached to the actin outer domains, presumably by binding to actin, tropomyosin, and troponin along the thin filaments [6]. One of the binding sites on subdomain 1 (orange residues, Figure 5A) involves the N terminus of F-actin, consistent with the observation that a nebulin fragment could be chemically crosslinked to this part of actin [31]. Reconstructions of F-actin decorated by a peptide containing a single actin binding module (S6R7 [13]) show additional density at this same site on subdomain 1 of actin (N.L., A.O., and E.H.E., unpublished data).

The existence of multiple nebulin binding sites on each actin subunit, taken together with the variable actin affinity of nebulin modules [12, 13], can explain the large range of stoichiometries previously observed between different nebulin fragments and actin. Fragments containing multiple actin binding modules may bind to actin, with only a subset of the modules actually bound to actin, and multiple fragments may also bind to the same actin subunit. The ND66 fragment that we have used derives from the single-repeat region at the C terminus of the nebulin molecule. Fragments from both the N- and C-terminal regions appear to bind to F-actin in a similar manner [6, 10]. However, three N-terminal fragments, which would be situated in the actomyosin overlap region of the sarcomere, bind to myosin and strongly inhibit actomyosin motility in a calcium- and calmodulin-sensitive manner, while ND66 and ND8 (another C-terminal fragment) do not bind to myosin and only weakly inhibit actomyosin motility [10]. One possibility, suggested by our observation of multiple binding sites, is that the pattern of binding of intact nebulin to F-actin varies over the length of the nebulin molecule, and this can account, at least in part, for functional differences between fragments from different regions of nebulin. This can be directly tested.

Regulation of vertebrate skeletal muscle contraction involves the troponin-tropomyosin complex within the actin-based thin filament. Tropomyosin sterically blocks actin's binding site for myosin in the relaxed state, and the binding of Ca^{2+} to troponin induces a movement by tropomyosin away from this blocked position [32]. An additional movement of tropomyosin (Figures 5A and 5B) occurs after the initial weak binding of myosin to actin [33–37]. A rotation of tropomyosin by ~35° around the axis of the actin filament [35] at the same time that a nebulin molecule is bound to actin raises many possibilities for steric clashes. It has been shown that a nebulin fragment can influence the interaction between actin and myosin heads [12]. Our observation that one site for nebulin binding (on subdomain 1) is in close proximity to both the strong binding site for myosin [38] and the blocked state of tropomyosin [35] suggests an interesting possibility: just as tropomyosin can move between different binding sites on F-actin, the intact nebulin molecule may "roll" on the surface of actin, either alone or in concert with tropomyosin. In this model, intact nebulin would symmetrically bind to every actin subunit (e.g., binding to subdomain 1 of every subunit) but could then move to a different position (e.g., binding to subdomain 4 of every actin). This model provides a testable framework for studying interactions between longer nebulin fragments and F-actin.

The existence of multiple nebulin binding sites on F-actin yields additional insights into the remarkable sequence conservation of actin. For example, there are no amino acid substitutions between chicken and human skeletal muscle actin. Some of this conservation must be due to the exquisite preservation across evolution of actin's helical parameters and internal modes of freedom [26]. A significant component of this conservation must also be due to the large number of proteins that interact with actin. When it is considered that proteins such as myosin [36, 39], tropomyosin [35, 40], ADF [18], and nebulin bind to more than one site on actin, the role of F-actin in the cell becomes even more remarkable.

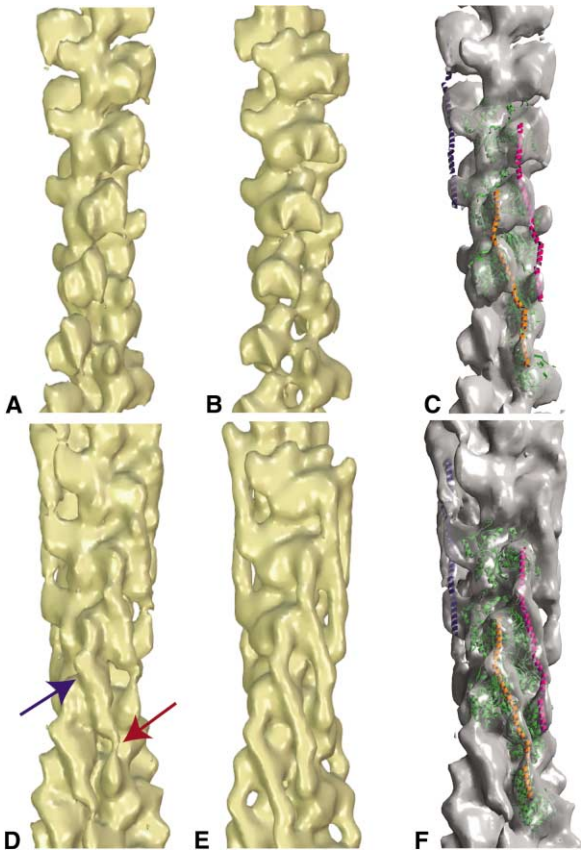

Figure 4. Reconstructions and a Model for the Complex

The actin-ND66 reconstruction is shown at 100% (A and C) and 200% (D and F) of the expected molecular volume, assuming one nebulin fragment per actin monomer and a partial specific volume of protein of 0.75 cm^3/gr. An atomic model for the actin-ND66 complex has been built into this reconstruction (C and F). There is an excellent fit between the actual reconstruction (A and D) and a 20 Å resolution rendered surface shown at either 100% (B) or 200% (E) of the expected volume. The nebulin fragments are represented as 104 residue α helices (blue, orange, and magenta), which bind to three separate sites on the actin subunit (green). This model accounts for most of the 128 residues contained within ND66 and spans the extra density present in the reconstruction. However, it may not be that all 128 residues are in an extended α-helical conformation, or residues at the ends of the fragment are disordered, or both. Differences from the model can be seen. The red arrow (D) indicates a region of weaker density in the actual reconstruction that may be simply due to the disorder of a single α helix spanning a gap. The blue arrow (D) indicates a region of greater density in the actual reconstruction that may be due to a more globular local fold.

Further insight into how other proteins bind to actin comes from a comparison between actin and actin's prokaryotic homolog MreB [41]. Six insertions exist in the actin sequence that are not present in MreB [41, 42]. Five of these insertions (40–48, 197–203, 262–274, 319–327, and 354–375) are likely to be involved in subunit-subunit contacts in the actin filament, including the "hydrophobic plug" contained within the loop 262–274 [43, 44]. A sixth insertion, residues 228–235, does not seem to be involved in such intrafilament interactions. Remarkably, this 228–235 insert appears to be part of the ND66 binding site in subdomain 4 of actin (Figure 5A). Additionally, the C-terminal insert in actin, residues 354–375, forms part of the binding site for ND66 in subdomain 1 of actin (Figure 5A). We suggest that these inserts may play an important role in both intrafilament interactions and interactions with many actin binding proteins, which can explain why all of these inserts have been stably incorporated into all actins over the entire range of eukaryotic evolution.

Experimental Procedures

Specimen Preparation and Electron Microscopy

Actin was prepared from rabbit skeletal muscle [45] and purified on a Superdex-200 column using the AKTA-Explorer system (Pharmacia, Uppsala, Sweden). G-Ca^{2+}-actin was converted to G-Mg^{2+}-actin by incubation of G-actin in 10 mM imidazol-buffer (pH 7.2), 0.2 mM ATP with 0.2 mM EGTA, and 0.2 mM $MgCl_2$. G-Mg^{2+}-actin was polymerized by 50 mM KCl at room temperature for 2 hr. Cloned nebulin fragment ND-66 (amino acid residues HNC 2594–2721, nucleotide 7789–8172 of HNC, accession number U35637) was prepared as described [6]. The ND66 sequence, with the conserved repeating residues in bold, is shown in Figure 6.

For experiments involving F-actin, 4 μM F-Mg^{2+}-actin was incubated with 40 μM ND-66 in 40 mM KCl, 10 mM imidazol-HCl (pH 7.2), 1 mM $MgCl_2$ for 7–12 min on ice. For experiments with ND66-induced polymerization of G-actin, 5 μM G-Mg^{2+}-actin was incubated with 50 μM ND-66 in 5 mM imidazol-HCl (pH 7.2), 0.2 mM ATP, 0.2 mM DTT (G buffer) on ice for 3 hr. These samples were then diluted two times by 40 mM KCl in G buffer. All samples were applied to lightly glow-discharged carbon-coated grids and stained with 1% uranyl acetate. Grids were examined in a Tecnai-12 (Phillips, Holland) electron microscope under minimal-dose conditions at an accelerating voltage of 80keV and a nominal magnification of 30,000×.

Image Analysis

Negatives were densitometered with a Leaf 45 scanner, using a raster of 3.9 Å/pixel. Most subsequent image processing employed the SPIDER software package [46]. Three-dimensional reconstructions were generated using the iterative helical real space reconstruction (IHRSR) method [17, 18, 20]. Images of filament segments were extracted into boxes of 100 × 100 pixels, corresponding to filament lengths of ~390 Å. Multireference crosscorrelation analysis was used to separate segments of undecorated actin filaments from decorated segments. An initial reconstruction was generated from the ND66-F-actin complexes, which showed additional mass when compared to a reconstruction of pure F-actin. However, heterogeneity existed in this initial reconstruction due to both incomplete binding by ND66 as well as the variable twist of F-actin. Reconstructions of both the ND66-decorated actin and pure F-actin were each regenerated 27 times with symmetries from 152°–179° rotation per subunit. Since each reconstruction was used to generate 90 reference projections (each related by a 4° azimuthal rotation about the helical axis), a total of 4860 (27 × 90 × 2) reference projections were used to sort the raw images, based upon both helical symmetry and whether ND66 was bound. The validation of this sorting procedure was that the reconstruction of the central subset (166° of rotation per subunit) of images selected as having a better crosscorrelation against the initial ND66-bound reconstruction showed an increased amount of additional mass, while a reconstruction from the corresponding symmetry peak of the images selected as having the better crosscorrelation against the pure F-actin showed no additional mass. This entire procedure was iterated, using the improved ND66-bound reconstruction each cycle as a reference volume. After five cycles, no further improvements in sorting were seen, and the solutions that were obtained were found to be stable.

Surface thresholds were determined by using 100% of the expected molecular volume for both undecorated actin and 1:1 ND66-actin complexes, assuming a partial specific volume of protein of 0.75 cm^3/g. The resolution in the IHRSR three-dimensional recon-

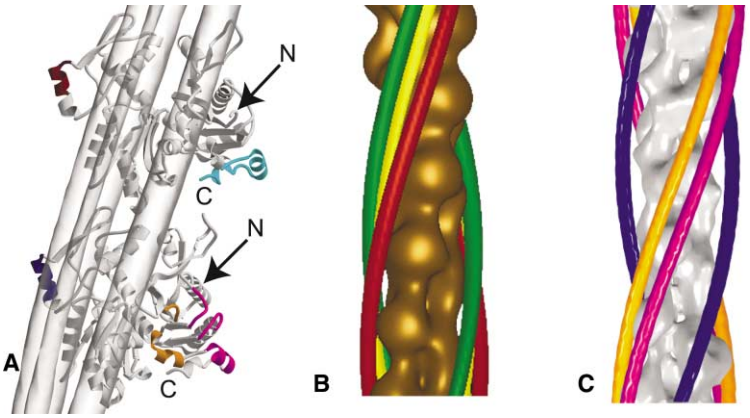

Figure 5. Models for Nebulin and Tropomyosin

(A) Ribbon representation of two actin monomers taken from the model for the actin-nebulin complex shown in Figures 4C and 4F. The N and C termini of actin are labeled. Residues proposed to interact with the nebulin fragment are colored magenta (96–101, 125–130, 359–366), blue (226–236), and orange (2–6, 348–356) in the lower actin subunit. Two insertions in the actin sequence that are not present in the bacterial MreB protein [41, 42] are shown in burgundy (228–235) and cyan (354–375) in the upper subunit. The location of three tropomyosin coiled coils on the actin subunits are indicated with transparent gray cylinders.

(B) Previously published model for three states of tropomyosin (green, yellow, and red) binding to F-actin [36].

(C) Model for the possible shift of full-length nebulin (blue, orange, and magenta) between the three observed nebulin binding sites in F-actin.

structions were estimated by dividing each data set into two arbitrary halves and generating reconstruction from each half set. Resolution was estimated by comparison of these half-set reconstructions, using both Fourier shell function correlation value of 0.5 and 3σ criterion. The resolution values were 33 Å and 22 Å, respectively. Filtrations of atomic models were made at different resolutions to best match the observed reconstruction (Figures 3B and 3E). A filter of $\sim$20 Å was found to most closely match the actual data, suggesting that 20–22 Å is the more reasonable estimate of true resolution. The statistical difference map was generated by dividing each data set (undecorated and decorated F-actin) into two halves, reconstructing each half, and estimating the variance in each map and in the difference map from these half sets.

Model Building

Manual fitting of the atomic structures for the actin monomer (PDB entry 2BTF) and a model α helix, generated using SYBYL (Tripos, Inc), into the 3D reconstruction of the F-actin:ND66 complex was done using the crystallography package O [47]. A 3D surface of the actin monomer, with resolution comparable to that of the F-actin:ND66 3D reconstruction, was first generated and docked into the EM reconstruction, using shape as the primary guide. The transformation used in docking the surface was then applied to the structure coordinates. A model of ND66 generated from α helices was then positioned into the EM reconstruction in areas not occupied by the actin monomer. Helical symmetry was imposed on the fitted structures to generate a model for the F-actin:ND66 filament.

Acknowledgments

This work was supported by National Institutes of Health AR42023 (to E.H.E.). We thank Roger Craig for Figure 5B, and we thank Anna-Lisa Pastore for an earlier gift of nebulin fragment S6R7.

Received: December 17, 2001
Revised: December 24, 2001

KE
PEMM**RVK**QT**Q**DHI**SSVKYKE**AI**G**QGTPIPDL
PEVK**RVK**ET**Q**KHI**SSVMYKE**NL**G**TGIPTTVT
PEIE**RVK**RN**Q**ENF**SSVLYKE**NM**G**KGTPLPVT
PEME**RVK**HN**Q**ENI**SSVLYKE**NV**G**KATATPVT
PE

Figure 6. ND66 Sequence, with the Conserved Repeating Residues in Bold

Accepted: December 24, 2001
Published: March 5, 2002

References

1. Wang, K., and Wright, J. (1988). Architecture of the sarcomere matrix of skeletal muscle: immunoelectron microscopic evidence that suggests a set of parallel inextensible nebulin filaments anchored at the Z line. J. Cell Biol. *107*, 2199–2212.
2. Wright, J., Huang, Q.Q., and Wang, K. (1993). Nebulin is a full-length template of actin filaments in the skeletal muscle sarcomere: an immunoelectron microscopic study of its orientation and span with site-specific monoclonal antibodies. J. Muscle Res. Cell Motil. *14*, 476–483.
3. Pelin, K., Hilpela, P., Donner, K., Sewry, C., Akkari, P.A., Wilton, S.D., Wattanasirichaigoon, D., Bang, M.L., Centner, T., Hanefeld, F., et al. (1999). Mutations in the nebulin gene associated with autosomal recessive nemaline myopathy. Proc. Natl. Acad. Sci. USA *96*, 2305–2310.
4. Tubridy, N., Fontaine, B., and Eymard, B. (2001). Congenital myopathies and congenital muscular dystrophies. Curr. Opin. Neurol. *14*, 575–582.
5. Labeit, S., and Kolmerer, B. (1995). The complete primary structure of human nebulin and its correlation to muscle structure. J. Mol. Biol. *248*, 308–315.
6. Wang, K., Knipfer, M., Huang, Q.Q., van Heerden, A., Hsu, L.C., Gutierrez, G., Quian, X.L., and Stedman, H. (1996). Human skeletal muscle nebulin sequence encodes a blueprint for thin filament architecture. Sequence motifs and affinity profiles of tandem repeats and terminal SH3. J. Biol. Chem. *271*, 4304–4314.
7. Labeit, S., Gibson, T., Lakey, A., Leonard, K., Zeviani, M., Knight, P., Wardale, J., and Trinick, J. (1991). Evidence that nebulin is a protein-ruler in muscle thin filaments. FEBS Lett. *282*, 313–316.
8. Kruger, M., Wright, J., and Wang, K. (1991). Nebulin as a length regulator of thin filaments of vertebrate skeletal muscles: correlation of thin filament length, nebulin size, and epitope profile. J. Cell Biol. *115*, 97–107.
9. Zhang, J.Q., Weisberg, A., and Horowits, R. (1998). Expression and purification of large nebulin fragments and their interaction with actin. Biophys. J. *74*, 349–359.
10. Root, D.D., and Wang, K. (1994). Calmodulin-sensitive interaction of human nebulin fragments with actin and myosin. Biochemistry *33*, 12581–12591.
11. Gonsior, S.M., Gautel, M., and Hinssen, H. (1998). A six-module human nebulin fragment bundles actin filaments and induces actin polymerization. J. Muscle Res. Cell Motil. *19*, 225–235.
12. Root, D.D., and Wang, K. (2001). High-affinity actin-binding nebulin fragments influence the actoS1 complex. Biochemistry *40*, 1171–1186.
13. Pfuhl, M., Winder, S.J., Castiglione Morelli, M.A., Labeit, S.,

and Pastore, A. (1996). Correlation between conformational and binding properties of nebulin repeats. J. Mol. Biol. *257*, 367–384.
14. Volkmann, N., DeRosier, D., Matsudaira, P., and Hanein, D. (2001). An atomic model of actin filaments cross-linked by fimbrin and its implications for bundle assembly and function. J. Cell Biol. *153*, 947–956.
15. Stokes, D.L., and DeRosier, D.J. (1991). Growth conditions control the size and order of actin bundles in vitro. Biophys. J. *59*, 456–465.
16. Sherman, M.B., Jakana, J., Sun, S., Matsudaira, P., Chiu, W., and Schmid, M.F. (1999). The three-dimensional structure of the limulus acrosomal process: A dynamic actin bundle. J. Mol. Biol. *294*, 139–149.
17. Egelman, E.H. (2000). A robust algorithm for the reconstruction of helical filaments using single-particle methods. Ultramicroscopy *85*, 225–234.
18. Galkin, V.E., Orlova, A., Lukoyanova, N., Wriggers, W., and Egelman, E.H. (2001). Actin depolymerizing factor stabilizes an existing state of F-actin and can change the tilt of F-actin subunits. J. Cell Biol. *153*, 75–86.
19. DeRosier, D.J., and Klug, A. (1968). Reconstruction of three-dimensional structures from electron micrographs. Nature *217*, 130–134.
20. Orlova, A., Galkin, V.E., VanLoock, M.S., Kim, E., Shvetsov, A., Reisler, E., and Egelman, E.H. (2001). Probing the structure of f-actin: cross-links constrain atomic models and modify actin dynamics. J. Mol. Biol. *312*, 95–106.
21. Yu, X., Jacobs, S.A., West, S.C., Ogawa, T., and Egelman, E.H. (2001). Domain structure and dynamics in the helical filaments formed by RecA and Rad51 on DNA. Proc. Natl. Acad. Sci. USA *98*, 8419–8424.
22. Yang, S., VanLoock, M.S., Yu, X., and Egelman, E.H. (2001). Comparison of bacteriophage T4 UvsX and human Rad51 filaments suggests that RecA-like polymers may have evolved independently. J. Mol. Biol. *312*, 999–1009.
23. Yang, S., Yu, X., Seitz, E.M., Kowalczykowski, S.C., and Egelman, E.H. (2001). Archaeal RadA protein binds DNA as both helical filaments and octameric rings. J. Mol. Biol. *314*, 1077–1085.
24. Orlova, A., Yu, X., and Egelman, E.H. (1994). Three-dimensional reconstruction of a co-complex of F-actin with antibody Fab fragments to actin's amino-terminus. Biophys. J. *66*, 276–285.
25. Hanein, D., Matsudaira, P., and DeRosier, D.J. (1997). Evidence for a conformational change in actin induced by fimbrin (N375) binding. J. Cell Biol. *139*, 387–396.
26. Egelman, E.H. (2001). Actin allostery again? Nat. Struct. Biol. *8*, 735–736.
27. Chik, J.K., Lindberg, U., and Schutt, C.E. (1996). The structure of an open state of β-actin at 2.65 Ångstrom resolution. J. Mol. Biol. *263*, 607–623.
28. Belmont, L.D., Orlova, A., Drubin, D.G., and Egelman, E.H. (1999). A change in actin conformation associated with filament instability after Pi release. Proc. Natl. Acad. Sci. USA *96*, 29–34.
29. Chen, M.J., Shih, C.L., and Wang, K. (1993). Nebulin as an actin zipper. A two-module nebulin fragment promotes actin nucleation and stabilizes actin filaments. J. Biol. Chem. *268*, 20327–20334.
30. Pfuhl, M., Winder, S.J., and Pastore, A. (1994). Nebulin, a helical actin binding protein. EMBO J. *13*, 1782–1789.
31. Shih, C.L., Chen, M.J., Linse, K., and Wang, K. (1997). Molecular contacts between nebulin and actin: cross-linking of nebulin modules to the N-terminus of actin. Biochemistry *36*, 1814–1825.
32. Huxley, H.E. (1972). Structural changes in the actin- and myosin-containing filaments during contraction. Cold Spring Harb. Symp. Quant. Biol. *37*, 361–376.
33. Maytum, R., Lehrer, S.S., and Geeves, M.A. (1999). Cooperativity and switching within the three-state model of muscle regulation. Biochemistry *38*, 1102–1110.
34. McKillop, D.F.A., and Geeves, M.A. (1993). Regulation of the interaction between actin and myosin subfragment-1: evidence for three states of the thin filament. Biophys. J. *65*, 693–701.
35. Vibert, P., Craig, R., and Lehman, W. (1997). Steric-model for activation of muscle thin filaments. J. Mol. Biol. *266*, 8–14.
36. Craig, R., and Lehman, W. (2001). Crossbridge and tropomyosin positions observed in native, interacting thick and thin filaments. J. Mol. Biol. *311*, 1027–1036.
37. Lehman, W., Hatch, V., Korman, V., Rosol, M., Thomas, L., Maytum, R., Geeves, M.A., Van Eyk, J.E., Tobacman, L.S., and Craig, R. (2000). Tropomyosin and actin isoforms modulate the localization of tropomyosin strands on actin filaments. J. Mol. Biol. *302*, 593–606.
38. Rayment, I., Holden, H.M., Whittaker, M., Yohn, C.B., Lorenz, M., Holmes, K.C., and Milligan, R.A. (1993). Structure of the actin-myosin complex and its implications for muscle contraction. Science *261*, 58–65.
39. DasGupta, G., and Reisler, E. (1991). Nucleotide-induced changes in the interaction of myosin subfragment 1 with actin: detection by antibodies against the N-terminal segment of actin. Biochemistry *30*, 9961–9966.
40. Lehman, W., Craig, R., and Vibert, P. (1994). Ca^{2+}-induced tropomyosin movement in *Limulus* thin filaments revealed by three-dimensional reconstruction. Nature *368*, 65–67.
41. van den Ent, F., Amos, L.A., and Lowe, J. (2001). Prokaryotic origin of the actin cytoskeleton. Nature *413*, 39–44.
42. Egelman, E.H. (2001). Molecular evolution: actin's long lost relative found. Curr. Biol. *11*, R1022–R1024.
43. Holmes, K.C., Popp, D., Gebhard, W., and Kabsch, W. (1990). Atomic model of the actin filament. Nature *347*, 44–49.
44. Kuang, B., and Rubenstein, P.A. (1997). Beryllium fluoride and phalloidin restore polymerizability of a mutant yeast actin (V266G,L267G) with severely decreased hydrophobicity in a subdomain 3/4 loop. J. Biol. Chem. *272*, 1237–1247.
45. Pardee, J., and Spudich, J. (1982). Purification of muscle actin. Methods Enzymol. *65*, 164–181.
46. Frank, J., Radermacher, M., Penczek, P., Zhu, J., Li, Y., Ladjadj, M., and Leith, A. (1996). SPIDER and WEB: processing and visualization of images in 3D electron microscopy and related fields. J. Struct. Biol. *116*, 190–199.
47. Jones, T.A., Zou, J.Y., Cowan, S.W., and Kjeldgaard, M. (1991). Improved methods for binding protein models in electron density maps and the location of errors in these models. Acta Crystallogr. A *47*, 110–119.
48. Millevoi, S., Trombitas, K., Kolmerer, B., Kostin, S., Schaper, J., Pelin, K., Granzier, H., and Labeit, S. (1998). Characterization of nebulette and nebulin and emerging concepts of their roles for vertebrate Z-discs. J. Mol. Biol. *282*, 111–123.
49. Bang, M.L., Mudry, R.E., McElhinny, A.S., Trombitas, K., Geach, A.J., Yamasaki, R., Sorimachi, H., Granzier, H., Gregorio, C.C., and Labeit, S. (2001). Myopalladin, a novel 145-kilodalton sarcomeric protein with multiple roles in Z-disc and I-band protein assemblies. J. Cell Biol. *153*, 413–427.